Focussed on Russian mechanics contributions for Structural Integrity

Visual Abstract

Finite-element study of residual stress distribution in Ti-6Al-4V alloy treated by laser shock peening with varying parameters

A. Kostina, M. Zhelnin, E. Gachegova, A. Prokhorov, A. Vshivkov, O. Plekhov
Institute of Continuous Media Mechanics of the Ural Branch of Russian Academy of Science, Russia
kostina@icmm.ru, http://orcid.org/0000-0002-5721-3301
zhelnin.m@icmm.ru, http://orcid.org/0000-0003-4498-450X
gachegova.e@icmm.ru, http://orcid.org/0000-0001-6849-9889
prokhorov.a@icmm.ru, https://orcid.org/0000-0002-6511-2105
vshivkov.a@icmm.ru, https://orcid.org/0000-0002-7667-455X
poa@icmm.ru, http://orcid.org/0000-0002-0378-8249

S. Swaroop
Vellore Institute of Technology, India
n.r.sathya.swaroop@gmail.com, http://orcid.org/0000-0001-9872-811X

ABSTRACT. Laser shock peening (LSP) is used to enhance surface quality of the metallic structures by the generation of compressive residual stresses on it. This work studies the effect of the main LSP parameters on residual stress fields by the finite-element method. The specimen under investigation is a square plate with a thickness of 3 mm made of Ti-6Al-4V. The performed analysis enhances understanding of LSP application to structures manufactured from this material and this information can be useful for a choice of optimal peening parameters. The effect of the spot size and shape, the pulse energy, the number of peen layers, overlapping of spots and temporal variation of the mechanical pressure induced by plasma is considered and analyzed. A 3D finite-element model based on the Johnson-Cook constitutive relation is developed and verified by the results of residual stress measurements performed for the LSP-treated samples under different conditions. From the obtained results the following main conclusions can be drawn: pulse energy provides the more significant effect although the resulting residual stresses profile tends to some saturation curve; temporal pressure pulse shape and its total duration also substantially alter the residual stress field; the least significant parameter is the spot shape.

KEYWORDS. Laser shock peening; Ti-6Al-4V; Hole drilling; Residual stress; FE analysis.

OPEN ACCESS

Citation: Kostina, A., Zhelnin, M., Gachegova, E., Prokhorov, A., Vshivkov, A., Plekhov, O., Swaroop, S., Finite-element study of residual stress distribution in Ti-6Al-4V alloy treated by laser shock peening with varying parameters, Frattura ed Integrità Strutturale, 61 (2022) 419-436.

Received: 27.05.2022
Accepted: 09.06.2022
Online first: 16.06.2022
Published: 01.07.2022

INTRODUCTION

Laser shock peening (LSP) is an effective non-contact method for surface treatment of metallic structures. During LSP short high-energy laser pulse generates shock waves which propagation induces compressive residual stresses. This process can be divided into four phases. Initially, laser pulse affects an opaque overlay (black paint or aluminum foil for example) applied to the surface of the structure immersed in confined media (water) and a thin (less than 1 μm) layer of the material is vaporized. In the second stage, steam continues to absorb the remaining laser energy which is ionized into plasma. In the third phase, a high-pressure mechanical impulse is generated due to the plasma expansion with its subsequent propagation into the material in the form of the elasto-plastic wave. In the last stage, the dynamical loading vanishes and residual stresses are induced by the inhomogeneous plastic strains formed during the third phase.
The main advantages of this approach in comparison with other surface treatment techniques are a high depth of penetration (more than 1 mm) and an ability to improve structures with complex geometry. LSP can be effectively applied to improve fatigue life, corrosion and wear resistance of metallic materials. For example, several works confirmed that LSP decreases fatigue crack propagation rate in aluminum samples [1-4]. In [5] was demonstrated that LSP increases corrosion resistance of AA2024-T3 aluminum alloy. Recently, C. Navarro et al. [6] have shown that LSP provides better fatigue properties of additive manufactured Ti-6Al-4V samples than other surface treatment techniques. However, to achieve better mechanical properties of the material it is necessary to apply suitable process parameters. In order to find optimal peening regime researchers investigate the effect of LSP parameters on the resulting stress field by finite-element analysis as well as by experimental studies. W. Braisted and R. Brockman [7] were the first who proposed an effective finite-element algorithm for the simulation of residual stresses which was based on the simultaneous use of the implicit and explicit time integration schemes. They considered one-sided and two-sided single LSP impact with round spot on Ti-6Al-4V and 35CD4 steel in a two-dimensional case and obtained a good correlation with experimental data. In [8] effect of laser power density, square focus size and temper stage on AA2198 aluminum alloy were experimentally studied. The authors have shown that these parameters significantly affect residual stress field. Based on the obtained results they proposed a numerical model which could predict the residual stress field for the considered temper stage and focus size. P. Peyre et al. [9] investigated surface deformation of 2050 aluminum alloy with different microstructure. A finite-element model was based on a single explicit analysis with 10^{-5} s intervals between pulses to obtain near-static equilibrium state. They successfully predicted velocity profiles measured by VISAR during LSP and obtained strain-rate sensitivity coefficient in Johnson-Cook constitutive law. Surface deformation induced by several impacts was in a good agreement with experimental data. However, residual stress field from a single impact was not predicted accurately. K. Langer et al. [10] found optimal LSP regimes with square spots to mitigate at-surface tensile residual stresses on a thin aluminum section by means of numerical simulation. A three-dimensional computational model was based on an explicit time integration scheme and the Johnson-Cook material model. Quasi-equilibrium state was achieved using Rayleigh damping. It was demonstrated that additional peen layers can suppress tensile stresses induced by the interaction of shock waves with geometry. In [11] residual stresses induced by single impact and multiple impacts LSP with round spots were predicted by explicit finite-element analysis with static damping. The obtained results showed similar trends with hole drilling measurements. M. Sticchi et al. [12] experimentally studied an effect of spot size and coverage for aluminum samples and the reinforced their findings with results of a two-dimensional explicit axisymmetric numerical model. They concluded that the most effective way to enhance the magnitude of compressive residual stress is to increase coverage. V. Pozdnyakov et al. [13] developed a two-step model which takes into account laser-matter-plasma-interaction. In the first step, temporal pressure profile is determined and then, it is applied in the second step as a boundary condition to obtain resulting residual stress field. It was shown that the proposed model can be applied to different coating materials and laser energies. In [14] special attention was paid to impact of overlapping in 2050-T8 aluminum alloy. This effect was studied by a combination of X-ray diffraction measurements with three-dimensional finite-element simulation. Temporal pressure profiles as well as yield strength were determined by VISAR and passed into a finite-element model as input data. Numerical scheme was based on a single explicit analysis for one and multiple shots. Heterogeneous surface residual stress distribution was obtained as a result of an LSP pattern with round overlapping spots. S. Golabi [15] developed LSP optimization technique based on Particle Swarm Optimization and finite-element simulation. Laser power, beam size and shape as well as peening pitch and pattern were chosen as optimization parameters while minimum compressive residual stresses and their depth acted as constraints. The analysis demonstrated that small round spots with a square pattern are optimal parameters for Inconel 718 alloy. Residual stresses were calculated using both explicit and implicit time integration schemes. Wang et al. [16] proposed a dislocation-based LSP model which can predict residual stresses along with grain refinement. They concluded that an increase in laser spot overlap ratio in Ti-6Al-4V (TC4) titanium alloy leads to the rise in penetration depth and grain refinement while for the same depth this results in an increase in compressive residual stresses. X. Zhang et al. [17] paid attention to studying residual stresses after two-sided LSP in Ti–

6Al–4V alloy plate with varying thickness. Three-dimensional numerical simulation was performed using dynamic and static steps combined with Johnson-Cook material behavior. LSP with a single round shot and multiple shots were considered and experimentally validated. As a result, it was found that for a thin specimen compressive residual stresses exist on both surfaces as well as in the middle of the specimen while for a thick specimen they occur only at the peened surface. Multiple impacts at the same location significantly increase magnitude of compressive residual stresses and their penetration depth. G. Xu et al. [18] studied an effect of scanning path and overlapping rate during LSP of 316L steel blade with square spots. Three overlapping rates of 30%, 50%, 70% were considered. Residual stresses were measured by X-ray diffraction technique and numerical simulation was based on explicit and implicit solutions. They obtained that an increase in overlapping rate contributes to a more uniform stress distribution. In [19] effect of stress drop at the center of the laser peened zone is studied. The authors used an explicit/implicit finite-element model with the Johnson-Cook constitutive equation to obtain surface displacement, stresses and strains in AISI 1045 steel after LSP with round and square spots. They explained lower compressive stresses at the center of the laser shock zone by reverse plastic loading due to the boundary effect of the impact. P. Mylavarapu et al. [20] made research on critical thickness which provides a negligible back reflection of stress waves in commercially pure aluminum. For this purpose, they developed a two-dimensional axisymmetric finite-element model and considered center circular laser impacts with various diameters. Full LSP process was simulated by an explicit time integration scheme. They found that critical thickness is 2.5 times higher than spot diameter. Also, they reported that a smaller spot diameter leads to tensile surface residual stress and a larger diameter induces higher depth of plastic deformation.

The above-mentioned studies have an important practical application as they help to understand an influence of LSP parameters on residual stress filed. However, they mainly focus on the surface treatment with round spots. As it was mentioned in [19] square laser shots can weaken or completely eliminate the problem of stress drop at the center of the peening zone. Therefore, this work mostly aims to enhance understanding of residual stress field distribution induced by LSP with multiple square shots in Ti-6Al-4V alloy. For this purpose, a three-dimensional numerical model based on Johnson-Cook constitutive relation was developed. As it was shown by the provided literature review, this equation gives reliable results and has a clear procedure for the identification of material constants. Material parameters for Ti-6Al-4V were obtained using results of dynamic experiments with strain rates in a range of 800 – 2200 s^{-1}. The model was verified by experimental data on LSP of square plate with a size of 70 mm and a depth of 3 mm. The central area of this plate was subjected to a series of shots without overlapping and resulting residual stresses were measured by the hole drilling method. After that, an effect of laser energy, its temporal variation, peening pattern and number of layers were studied with the objective to obtain better insight into their influence on the residual stress filed.

EXPERIMENTAL PROCEDURES

Material and components

In the present study, the laser shot peening technique was applied to induce residual stress in samples of Ti-6Al-4V titanium alloy, which is widely used in the aircraft industry. The chemical composition of the Ti-6Al-4V alloy is given in Tab. 1. The samples peened in the experiment were a square plate form. The thickness of the plate was 3 mm and its side size was 70 mm.

Composition	V	Al	Sn	Zr	Mo	C	Si	Cr	Ni	Fe	Cu	Nb	Ti
Percent (%)	4.22	5.48	0.0625	0.0028	0.005	0.369	0.0222	0.369	<0.0010	0.112	<0.02	0.0386	90.0

Table 1: Chemical composition of Ti-6Al-4V titanium alloy (%).

The main component of the laser peening system used in the experiment is a solid-state laser Nd YAG SGR - extra - 10 manufactured by Beamtech (Fig.1 (a)). The device can produce a laser pulse with a maximum duration of 10 ns and energy of 10 J. The wavelength and the maximal frequency of the laser beam are 1064 nm and 5 Hz.

The laser peening system is equipped with three types of optic lenses, which allow transforming a laser beam into a shape of a square with a side of 1mm and 3 mm, and a circle with a radius of 2 mm. By tuning the laser beam shape and the pulse energy, the power density of one laser pulse can be variated from 1 GW/cm² to 90 GW/cm².

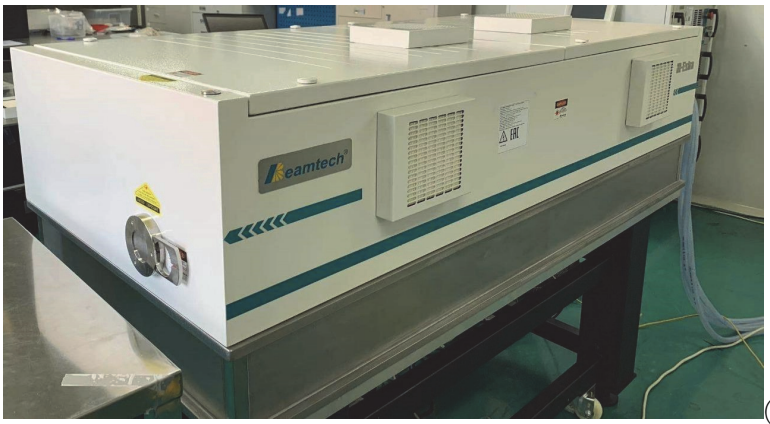

(a)

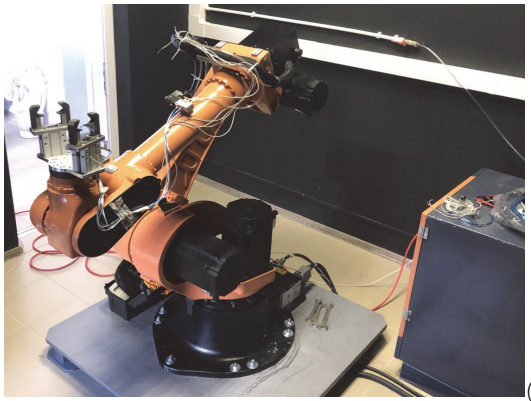
(b)

Figure 1: (a) The Nd YAG laser SGR - extra - 10 manufactured by Beamtech; (b) the robotic manipulator SR50 manufactured by STEP.

Another essential component of the laser peening system is a robotic manipulator SR50 manufactured by STEP (Fig.1 (b)). During the laser peening process, the manipulator controls the location of the sample that allows treating the sample surface with high accuracy. The precision of the position is 0.2 mm and a maximum weight of a tested sample is 50kg. The motion speed of this manipulator is in a range of 0.1mm/s to 500mm/s. The manipulator moves the sample according to a programmed path. As soon as the desired area of the surface is located in front of the laser, a pulse is generated and the sample surface is subjected to impact loading. The process is finished as a desired number of laser pulses is achieved.
It is possible to generate various designs of distributions of residual stress using different optical lenses, laser spot overlaps, and laser pulse power.

LSP experiment

In the experiment, Ti-6Al-4V alloy samples were subjected to one-sided laser peening. The processed area was a square region with a side of 12 mm. The surface treatment was conducted for several power densities of laser pulse which were equal to 3.3 GW/cm^2, 20 GW/cm^2, 30 GW/cm^2, 40 GW/cm^2. The number of laser pulses for each power density was defined by the spot size which was equal to 3 mm for 3.3 GW/cm^2 and 1 mm for 20 GW/cm^2, 30 GW/cm^2, 40 GW/cm^2. Before the peening, the processed area was covered with aluminium foil to reduce its destruction. Then the sample is fixed by the grips of the manipulator and located on the front of the laser. On the surface of the sample with aluminium foil the absorption water layer is additionally applied. The water layer is important to increase the plasma pressure and generate high impact loading on the sample surface. After each laser pulse, the sample is moved to the next position according to the path established for the manipulator by the user-defined program.

Hole drilling method for residual stress measurements

Residual stress analysis plays an important role in the mechanical design stages. In terms of cost, accuracy, and versatility, one of the most effective non-destructive methods of residual stress relief is the hole-drilling method.

This involves drilling a small hole (usually 1.8-2.0 mm) at high speed in order to induce a change in the stress state associated with the change and redistribution of stresses within the specimen. A Three-Element Clockwise Hole-Drilling Rosette is placed on the surface of the specimen and a hole is drilled at a defined location. Drilling is carried out in steps, at the end of each step the strain values of the hole are recorded with the strain gauge. High-speed drilling does not change the stress state of the material, so it is possible to drill the hole without inducing new stresses, which is essential for a complete test. The measurement error is less than 1 μm/m. From the data obtained, the inverse problem is solved, resulting in a residual stress profile.
All measurements are carried out in accordance with the worldwide standard ASTM E 837-13 "Standard Test Method for Determining Residual Stresses by the Hole-Drilling Strain Gage Method".

LASER SHOCK PEENING SIMULATION

Mathematical model of stress wave propagation

In the laser peening process, stress waves are induced in the target material. The mathematical description of the stress waves propagation is based on the momentum conservation law and constitutive relations which provides a relationship between stress and strain fields.
If the effect of gravity is neglected, the equation of the motion is written based on the momentum conservation law as

$$\mathrm{div}\boldsymbol{\sigma} = \rho \frac{\mathrm{d}^2\mathbf{u}}{\mathrm{d}t^2}, \tag{1}$$

where t is time, $\boldsymbol{\sigma}$ is Cauchy stress tensor, ρ is density of the target material, $\mathbf{u}$ is the displacement vector.
The total strain $\boldsymbol{\varepsilon}$ is determined by the displacement vector $\mathbf{u}$ from the small strain approximation as

$$\boldsymbol{\varepsilon} = \frac{1}{2}\left(\mathrm{grad}\mathbf{u} + \mathrm{grad}\mathbf{u}^T\right). \tag{2}$$

According to the principle of additive decomposition, the increment of the total strain $\mathrm{d}\boldsymbol{\varepsilon}$ can be expressed through the increments of the elastic strain $\mathrm{d}\boldsymbol{\varepsilon}^{el}$ and the plastic strain $\mathrm{d}\boldsymbol{\varepsilon}^{pl}$ as

$$\mathrm{d}\boldsymbol{\varepsilon} = \mathrm{d}\boldsymbol{\varepsilon}^{el} + \mathrm{d}\boldsymbol{\varepsilon}^{pl}. \tag{3}$$

In the case of the isotropic material the Cauchy stress $\boldsymbol{\sigma}$ is determined through the Hook's law as

$$\boldsymbol{\sigma} = \lambda\, \varepsilon_{vol}^{el}\mathbf{I} + 2\mu\boldsymbol{\varepsilon}^{el}, \tag{4}$$

where $\mathbf{I}$ is the identity tensor, ε_{vol}^{el} is the volumetric part of the elastic strain, λ, μ are Lame parameters, which can be estimated from Young modulus E and Poisson ratio ν.
On the basis of the associated flow theory of plasticity the rate of the plastic strain can be determined as

$$\mathrm{d}\boldsymbol{\varepsilon}^{pl} = \mathrm{d}\lambda \frac{\partial F}{\partial \boldsymbol{\sigma}}, \tag{5}$$

where $\mathrm{d}\lambda$ is the plastic multiplier given by the Prager condition, F is the yield surface.
In the case of the isotropic hardening the yield surface can be written as

$$F = \sigma_{eq} - \sigma_y(\varepsilon_{eq}^{pl}), \tag{6}$$

where σ_{eq} is the equivalent stress, ε_{eq}^{pl} is the equivalent plastic strain, $\sigma_y = \sigma_y(\varepsilon_{eq}^{pl})$ is a function which determines current value of the yield limit.

Mathematical model for plastic strain

For a generation of the residual stress in the target material, the plastic deformation should be induced by the laser shot during peening. This impact loading can lead to a very high strain rate hardening effect of the target material. To characterize the dynamic response with acceptable accuracy the Johnson-Cook material model is frequently employed [10]. The model allows capturing strain hardening, strain rate, and thermal effects in a material subjected to an impact loading. Also, the parameters of the model responsible for each effect can be separately identified and the model is incorporated in the most engineering packages for finite element simulation. As the laser peening can be considered as a fully mechanical process [21], the thermal effect can be avoided. In this case, the material model is written as

$$F = \sigma_{eq} - \left[A + B\left(\varepsilon_{eq}^{pl}\right)^{n} \right] \left[1 + C \ln \frac{\dot{\varepsilon}_{eq}^{pl}}{\dot{\varepsilon}_0} \right], \tag{7}$$

where $\dot{\varepsilon}_{eq}^{pl}$ is the equivalent plastic strain rate, $\dot{\varepsilon}_0$ is a reference plastic strain rate, A, B, C, n is material parameters. The reference plastic strain rate $\dot{\varepsilon}_0$ is in the range of quasi-static tests. The parameter A corresponds to the initial value of the yield limit in the quasi-static test. The parameters B, n describe strain hardening. The parameter C is responsible for the strain rate sensitivity.

In the present study identification of the parameters of the Johnson-Cook model was carried out based on stress-strain curves obtained in a series of quasi-static and dynamical tests of Ti-6Al-4V for strain rates of $5 \cdot 10^{-3}$ – $2.2 \cdot 10^{3}$ s^{-1}.

In the first step, the Young modulus and the offset yield strength of the material were determined from the elastic part of the deformation diagrams. After that, the strain hardening part was extracted by subtraction of the elastic strain from the total strain. The elastic properties and the density of Ti-6Al-4V are shown in Tab. 2. The parameters A, B, n were identified on the plastic part of the deformation diagrams provided by the quasi-static tests. To determine the parameter C, the stress-strain curves measured in split-Hopkinson-bar testing were used.

Identification of the material parameters was performed by fitting the experimental data by analytical curves given by Eq. (7) according to the least square method. To solve the corresponding optimization problem, a procedure based on the True Region Reflective algorithm provided by the SciPy module was developed. The values of the determined parameters were constrained to be positive. Initial values of the determined parameters were given according to data listed in the existing literature [22-24]

The identified parameters of the Johnson-Cook model are listed in Tab. 3. Fig. 2 shows the comparison between analytical curves calculated from Eq (7) with the determined parameters and experimental data. It can be seen that the analytical predictions are close to the measured response of the material on the dynamical loading. The identified parameters of Ti-6Al-4V are close to the values presented in [22-24].

E [GPa]	ν	ϱ [kg/m^3]
106.7	0.314	4424

Table 2: Elastic parameters and density.

A [МПа]	B [МПа]	n [1]	C [1]	$\dot{\varepsilon}_0$ [1/s]
978	826	0.639	0.034	0.005

Table 3: Johnson-Cook material parameters.

Pressure model

Following [7-8], [11], [14], [17], [25] in the present study LSP simulation considered as a purely mechanical process, and all effects related to plasma generation and material vaporization are disregarded. The stress waves are disturbed by the pressure pulse, which is applied to the boundary of the sample subjected to the laser peening. In the most general case pressure is spatially and temporally non-uniform. However, for square laser spot it is usually assumed uniform spatial distribution of

the pressure [8], [18-19]. At the same time, in several works [14], [26-28] it is assumed to decrease in amplitude with an increase in distance from the center of the shot during LSP with round spots. Typically, temporal non-uniformity is taken into account by approximation of the pulse by a triangular shape [7], [16], [25], Gaussian distribution [10], [28] and linear piece-wise interpolation [11], [22], [29]. In this work the simplified triangular pulse was used.

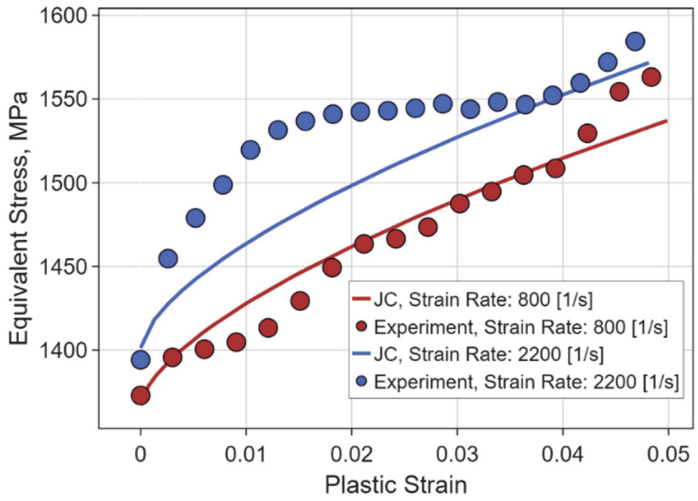

Figure 2: Equivalent stress vs plastic strain obtained for strain rates of 800 1/s (red color) and 2200 1/s (blue color) (solid lines are numerical results; markers are the experimental data).

In general, the duration of the pressure loading induced by plasma is several times higher than laser pulse impact [16]. In this work, the laser pulse duration τ was equal to 10 ns. The whole duration of the loading and peak loading time were calibrated according to the experimental data on residual stress profiles and equal to 80 ns and 20 ns, respectively. Therefore, the laser energy was amplified linearly to the peak value within the first 20 ns and then decreased linearly to zero from 20 ns to 80 ns:

$$P(t)=\begin{cases}\dfrac{t}{2\tau}P_{peak}, & 0\le t<2\tau,\\ \dfrac{8\tau-t}{2\tau}P_{peak}, & 2\tau\le t\le 8\tau\end{cases}. \tag{8}$$

The peak pressure value P_{peak} is calculated according to the confined ablation model proposed by R. Fabbro et al. [30]. In compliance with this work, the value P_{peak} induced by LSP can be calculated as

$$P_{peak}=0.01\sqrt{\frac{\alpha}{2\alpha+3}\cdot Z\cdot I}\,, \tag{9}$$

$$Z=\frac{2\cdot Z_{water}\cdot Z_t}{Z_{water}+Z_t}, \tag{10}$$

$$I=\frac{P_{pulse}}{S}, \tag{11}$$

where α is the efficiency coefficient (typically, α = 0.33), Z_{water} and Z_t are the acoustic impedances of water (Z_{water} = $0.17\cdot10^6$ [g/(cm²·s)]) and the target material (Z_t = $2.75\cdot10^6$ [g/(cm²·s)] [16]), P_{pulse} is the pulse power, S is the area of the laser spot.

Computational model

A three-dimensional finite-element model for residual stress prediction based on the equation of motion (1) along with relations (2-7) was developed in the finite element software ABAQUS. Geometry of the considered area has a square shape with a thickness of 3 mm. The central zone located on the upper boundary of the plate was subjected to LSP treatment. The opposite boundary was fixed.

The mechanical response of a sample on each impact loading produced by the laser pulse was modeled through two steps. The first solution step is dynamic analysis. At this step plastic deformation caused by stress waves propagation is calculated by solving the equation of motion (1) supplemented by the Johnson-Cook relation (7). Time variation of the pressure pulse acting on the LSP-treated zone is prescribed by Eqn. (8) with the peak pressure estimated by (9). The computation of the stress waves propagation ends when no further plastic deformation occurs. The duration of the period was about 10 μs. Simulation for dynamical analysis was performed using the explicit time integration. The second solution step is static analysis. An implicit solver was employed for this purpose. At this step, residual stress associated with the plastic deformation determined in the dynamic analysis is estimated by solving the static equilibrium equation. The equation corresponds to the equation of the motion (1) with zero inertial term. At the start moment of the static analysis distributions of stress, strain, and displacement fields are given by transferring from the end of the dynamic analysis. The peened boundary of the sample is supposed to be free from the loading and displacement constraints. Thus, residual stress induced by one laser pulse was determined by one pair of analysis. For the further laser pulse, the estimated residual stress was considered as the initial condition for the subsequent dynamic analysis. Both analyses were carried out using one computational mesh consisting of 8-node linear brick elements with reduced integration (C3D8R). In the laser peened region the mesh was refined in vertical and horizontal directions. The in-depth element size in this zone was set to 0.1 mm, while in-plane elements had a size of 0.15 mm. According to [9], [11], [25], such mesh provides accurate calculation of residual stress field and stress wave propagation. A coarser mesh with a size varying from 1.5 mm to 5 mm was used to spatial discretization in the remaining domain. Time or load stepping was performed automatically by the software.

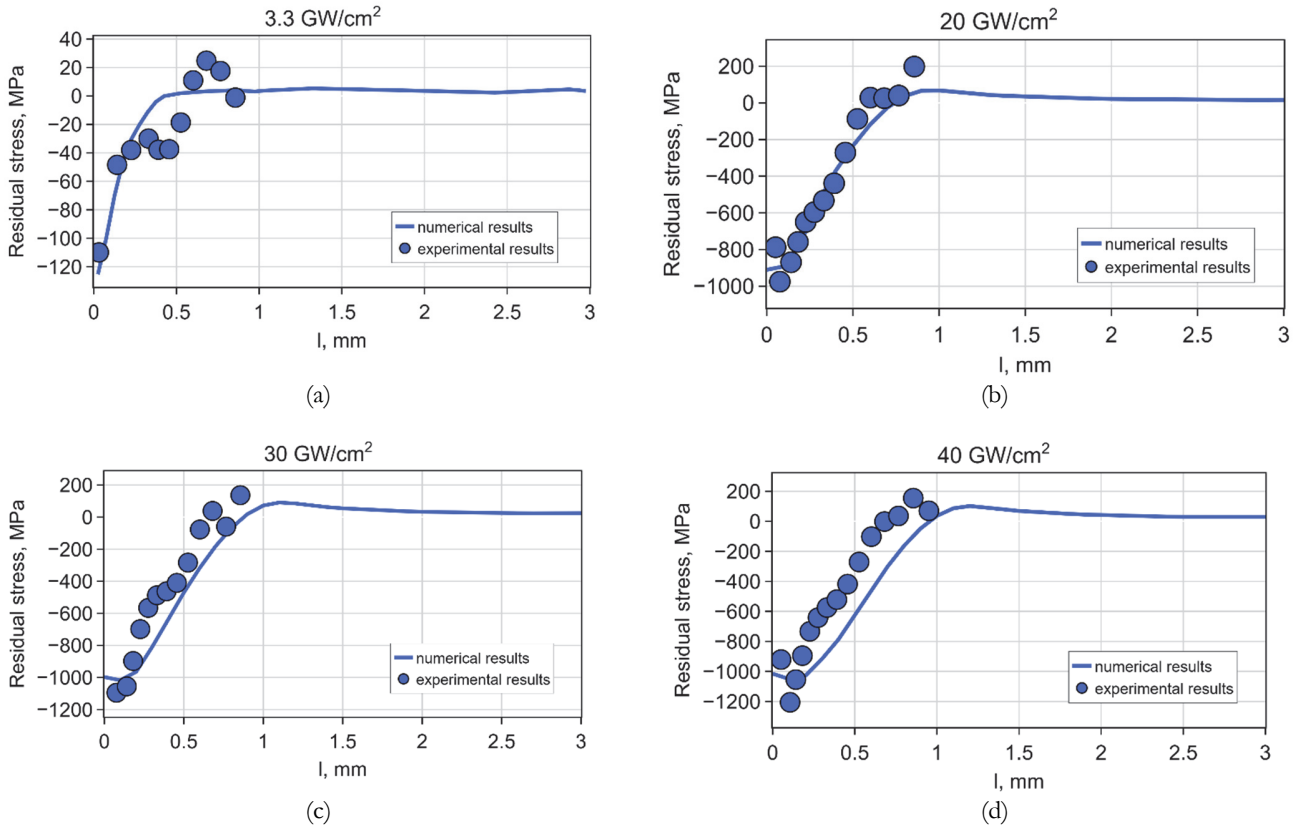

Figure 3: In-depth residual stress profiles obtained by LSP with a peak intensity equal to: (a) 3.3 GW/cm² (3.1 GPa), (b) 20 GW/cm² (7.6 GPa), (c) 30 GW/cm² (9.3 GPa), (d) 40 GW/cm² (10.7 GPa), (markers are the experimental data, solid lines are the numerical results).

Model verification

The above-described model was used to predict residual stresses in Ti-6Al-4V titanium square samples with a size of 70 mm and compared with experimental data for different laser intensities. The central part of the surface was peened with a series of square laser spots without overlapping. Residual stresses were measured by the hole drilling method. The details of the LSP experiments are given above.

Fig. 2 shows the results of the simulation for different power densities together with the experimental data. The study compares residual stresses for 3.3 GW/cm², 20 GW/cm², 30 GW/cm², 40 GW/cm² peak intensities which according to (9) are equivalent to 3.1 GPa, 7.6 GPa, 9.3 GPa, 10.7 GPa respectively. The FE results were obtained by averaging the residual stresses over the circle with a radius equal to the hole radius (0.9 mm) at several depths of the sample. The location of the circle corresponded to the drilling site. It should be noted that the measured residual stresses at the peened surface and close to the peened surface are excluded because of the possible measurement inaccuracies of the hole drilling method for the initial steps close to the peened surface. As it can be seen, calculated residual stresses are in a reasonable agreement with the experimental data under different LSP conditions. For the largest peak laser intensity (40 GW/cm²) (Fig. 3 (d)) the numerical model predicts deeper compressive residual stress penetration depth than the experimental data. This can be explained by the surface damage in LSP experiments without protective layer. Despite the polishing of the surface after LSP which removes tensile residual stresses, the surface damage resulting from high power densities prevents deeper propagation of the compressive residual stress into the sample during treatment. Therefore, penetration depths for 30 GW/cm² (Fig. 3 (c)) and 40 GW/cm² (Fig. 3 (d)) are nearly the same and slightly more than 0.5 mm. On the contrary, the model predicts an increase in the penetration depth with the rise in peak intensity. It is equal to 0.8 mm and 1 mm for the intensities of 30 GW/cm² and 40 GW/cm² respectively. The experimental data also show higher tensile residual stress for all considered cases. This can be due to some initial tensile stresses in the specimen before LSP which are not considered in the simulation. Overall, the results show that an increase in peak power density leads to the growth in the minimum value of compressive residual stress. The model successfully describes this pattern and therefore can be used for LSP simulation.

RESULTS AND DISCUSSIONS

The choice of the optimal peening regime is an important problem for the aircraft industry. LSP parameters should be selected in such way that they can provide as deeper compressive residual stresses as possible. However, the variability of the possible parameters is restricted by the characteristics of the used laser. In this section, we will apply the developed model to the numerical investigation of the residual stresses obtained by laser peening with different patterns. Numerical simulation does not require a use of the expensive consumables and therefore, is more suitable for this task than experimental study.

To reduce calculation time, we decrease the treatment area to a square of 6x6 mm. The center of the peening area corresponds to the center of the sample. In all sections of this paragraph, residual stress profiles are averaged over the whole peening zone at several depths with a step of 0.1 mm. The effects of the following LSP parameters are investigated: spot size and shape, number of peen layers, pulse energy, overlapping and temporal variation of the pressure pulse. The obtained information can enhance understanding of LSP application to structures made of Ti-6Al-4V titanium alloy and select the peening regime for the used laser.

Effect of spot size

In this section, we analyze the effect of the spot size on residual stress obtained by LSP with a peak intensity equal to 10 GW/cm² which is equivalent to 5.37 GPa according to (9). Here and below, the temporal pressure profile is described by (8), unless otherwise is stated. The peening pattern consists of a series of successive square shots without overlapping made line by line.

Fig. 4 shows the distribution of the stress component σ_{11} over the volume of the sample with sizes of 6x6x3 mm which corresponds to the treated region for square spots of 3 mm (Fig. 4 (a)) and 1 mm (Fig. 4 (b)). The distribution of σ_{22} component is similar, since equi-biaxial stress field is assumed in the numerical simulation. Therefore, here and further only one stress component is presented. The results show that near the peened surface of the sample a favorable zone with compressive residual stresses is formed in both cases. The distributions are non-uniform and have periodic structures for both focus sizes.

In the center of each shot, a stress drop can be seen, which is illustrated a so-called "residual stress hole" effect [19]. This phenomenon is attributed to the generation of the surface release waves from the perimeter of the laser spot and its focusing

at the spot center. As a result, the compressive residual stress at the center has a smaller magnitude than residual stresses at the perimeter [17-18]. The main difference between the results is observed on the peened surface of the sample. Due to the larger size, the square spot of 3mm results in a more homogeneous compressive residual stress distribution on the surface. However, the minimum value of the residual stress is reached on the surface in both cases.

The resulting in-depth stress profiles are shown in Fig. 5. It can be seen that the larger focus size induces a lower value of the compressive residual stress at the surface which corresponds to the stress distribution shown in Fig. 4. For the square spot of 1 mm the minimum value is -700 MPa while for 3 mm pulse this value is -800 MPa. Thus, the rise in magnitude is 14%. Moreover, the application of larger spots leads to an increase in penetration depth. The pulse of 1 mm is characterized by the penetration depth of 0.6 mm and 3 mm pulse increases the depth up to 0.8 mm. In addition, LSP with the spot of 1 mm induces higher tensile residual stress within the volume of the material at the same time for the spot of 3 mm tensile residual stress is negligible. It is interesting to note that LSP treatment with 3 mm square pulse is accompanied by slight compressive residual stress on the opposite side of the specimen. That also beneficially affects the durability of the treated material.

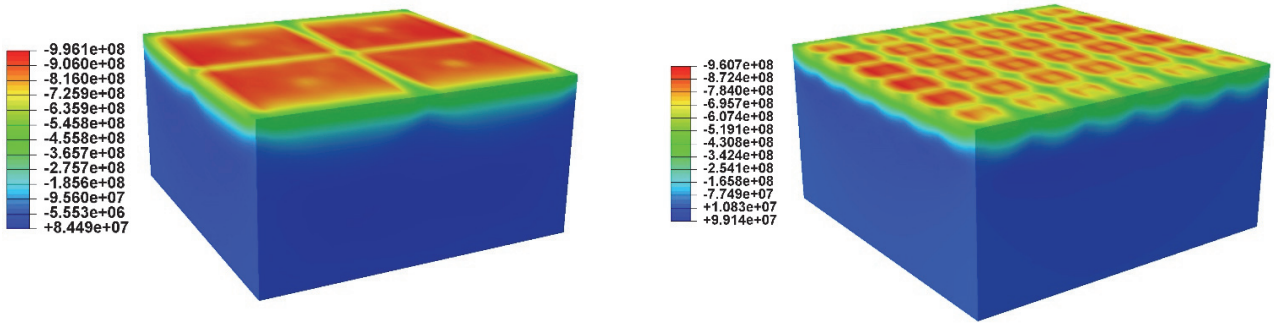

(a) (b)

Figure 4: Residual stress distribution over the peened area with adjacent volume of the sample obtained by LSP with a peak intensity equal to 10 GW/cm² for square pulse: (a) 3 mm, (b) 1 mm.

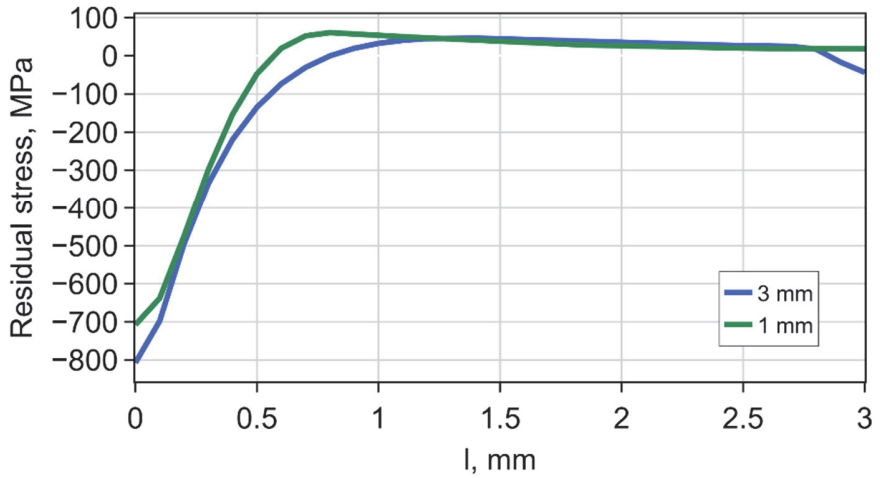

Figure 5: In-depth residual stress profiles obtained by LSP with square pulses of different sizes and peak intensity of 10 GW/cm² (blue line is the size of square equal to 3 mm, green line is the size of square equal to 1 mm).

Effect of pulse energy

This section is devoted to the study of the laser pulse energy effect on the in-depth residual stress obtained by multiple LSP with square pulses of 3 mm. LSP strategy is the same as the one described in the previous section for the identical pulse size. Three different energies are analyzed: 5 J (5.5 GW/cm²), 7 J (7.8 GW/cm²), 9 J (10 GW/cm²). In accordance with (9), these energies are equivalent to 4 GPa, 4.8 GPa and 5.37 GPa.

Fig. 4 (a) illustrates the distribution of residual stress over the peened area of the sample and the adjacent volume for 9 J (10 GW/cm²). For other considered power densities, the distributions are qualitatively similar.
In-depth residual stress profiles for the studied pulse densities are in Fig. 6. It can be seen, that an increase in laser energy leads to a growth in minimum compressive residual stress at the peened surface of the sample. On the whole, the higher is the energy the lower value of the compressive residual stress. The rise in the energy from 5J (5.5 GW/cm²) to 7 J (7.8 GW/cm²) results in the enhancement of the magnitude by 70% from -400 MPa to -680 MPa. Further increase in energy doesn't show such significant improvement. The value of the residual stress drops only to -800 MPa (18%) when energy is increased from 7 J (7.8 GW/cm²) to 9 J (10 GW/cm²). Therefore, from a certain value of the pulse energy, the growth rate of the compressive residual stress magnitude decreases. This conclusion is confirmed by the data presented in Fig. 3 for the square spot of 1 mm. The increase in the power density from 20 GW/cm² to 30 GW/cm² doesn't lead to a substantial diminishing of the residual stress value.
Fig. 6 also demonstrates, that the penetration depth of compressive residual stress increases with the rise in the pulse energy. For 5J (5.5 GW/cm²) pulse it is equal to slightly more than 0.5 mm, for 7 J (7.8 GW/cm²) pulse it is about 0.7 mm and for 9 J (10 GW/cm²) pulse it is 0.8 mm. Hence, the influence of the pulse energy on the penetration depth also diminishes. In addition, the rise in the pulse energy doesn't induce significant rise in tensile residual stress within the volume of the specimen. Compressive residual stress at the side opposite to the peened area is nearly zero for the pulse energy of 5J (5.5 GW/cm²). At the same time, for the pulse energies of 7 J (7.8 GW/cm²) and 9 J (10 GW/cm²) a slight compressive residual stress around -50MPa is observed.

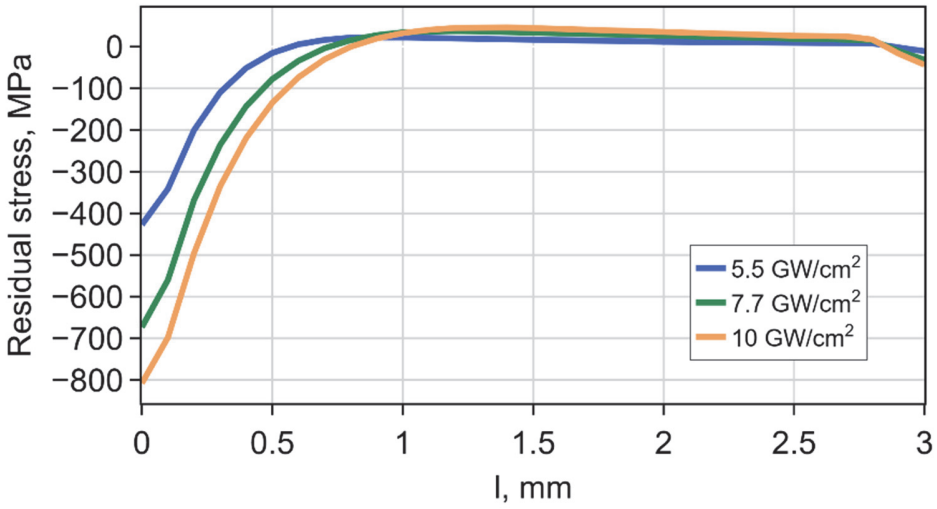

Figure 6: In-depth residual stress profiles obtained by LSP with different pulse energy and square pulses of 3 mm (blue line is the peak intensity of 5.5 GW/cm², green line is the peak intensity of 7.7 GW/cm², orange line is the peak intensity of 10 GW/cm²).

Effect of peen layers

An increase in the number of peen layers can also gain the magnitude of compressive residual stresses. Fig. 7 presents in-depth residual stress profiles for one, two and three peen layers obtained with the peak intensity of 10 GW/cm² and square pulse of 3 mm. It can be seen that additional layers increase the magnitude of compressive residual stress. However, the value of the increment is not the constant and gradually declines with each additional layer. For the first peen layer the minimum value at the peened surface is -800 MPa. The laser peening by the second layer drops it to about -890 MPa, which is 11.2% lower than the value for the first layer. The minimum value for the third layer is around -930 MPa. That indicates a decrease of the minimum value in 4.5% compared to the two peen layers.
Fig. 7 illustrates that additional peen layers improve the penetration depth of compressive residual stress. Its value for the first layer is 0.8 mm and it is 1 mm and 1.15 mm for the second and third layers, respectively. Consequently, adding the second peen layer can gain both the penetration depth and magnitude of compressive residual stress while adding the subsequent layers does not lead to the significant improvement of LSP results. It should be noted also, that tensile residual stress in the mid-depth plane of the sample increases slightly with each extra layer. At the same time, compressive residual stress at the side opposite to the peening surface does not change.
The made observations along with the result presented in the previous section allow assuming that the minimum compressive residual stress tends to saturation. It means that from a certain value of the pulse energy and a number of the

peen layers there is no significant influence of these LSP parameters on the minimal value of compressive residual stress and its penetration depth.

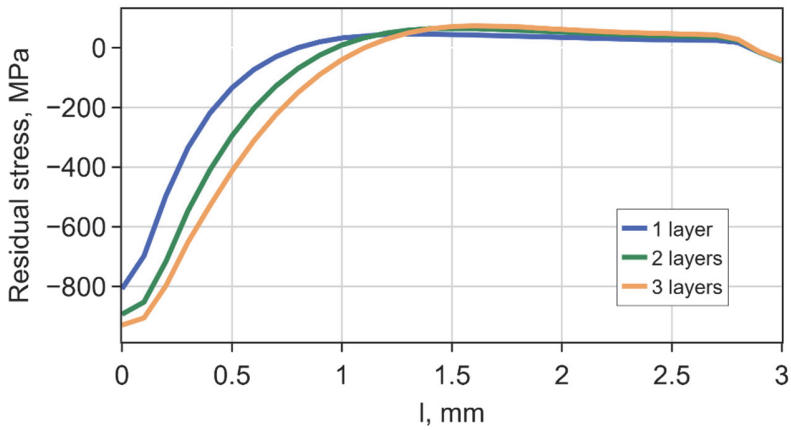

Figure 7: In-depth residual stress profiles obtained by LSP with different number of layers, square pulses of 3 mm and peak intensity of 10 GW/cm² (blue line is the one peen layer, green line is two peen layers, orange line is three peen layers).

Effect of overlapping

In this section, an effect of spot overlapping is investigated. The area of interest is treated by LSP with a peak intensity equal to 10 GW/cm² and square spots of 3 mm. Peening strategy of the sample with 50% overlapping is made successively in three rows, line by line. So, the total number of shots is nine. The resulting compressive residual stresses are compared with those obtained with no overlapping.

Fig. 8 (a) displays the distribution of the residual stress field over the volume of the sample with the sizes of 6x6x3 mm which includes the peened surface and the adjacent material. A comparison of Fig. 8(a) and Fig. 4 (a) shows that residual stress is distributed more uniformly when LSP is performed with 50% overlapping. On the whole, the values of the compressive residual stress on the peened surface of the sample with 50% overlapping are lower than without overlapping. When pressure induced by a laser shot is superimposed on the existing compressive stress field generated by the previous shot, the compressive stress magnitude increases. In-depth residual stress profiles presented in Fig. 8(b) confirm this statement. The graphs show that the overlapping leads to a decline of the minimum value of 7.5% from -800 MPa to -860 MPa. This effect is accompanied by a minor increase in tensile residual stress in the mid-depth plane of the sample. The penetration depth of the compressive residual stress increases from 0.8 mm to 1.1 mm. At the side opposite to the peened surface compressive residual stress slightly decrease. Overall, overlapping positively affects peeing results leading to higher penetration depth and decreasing the minimum value of compressive residual stress.

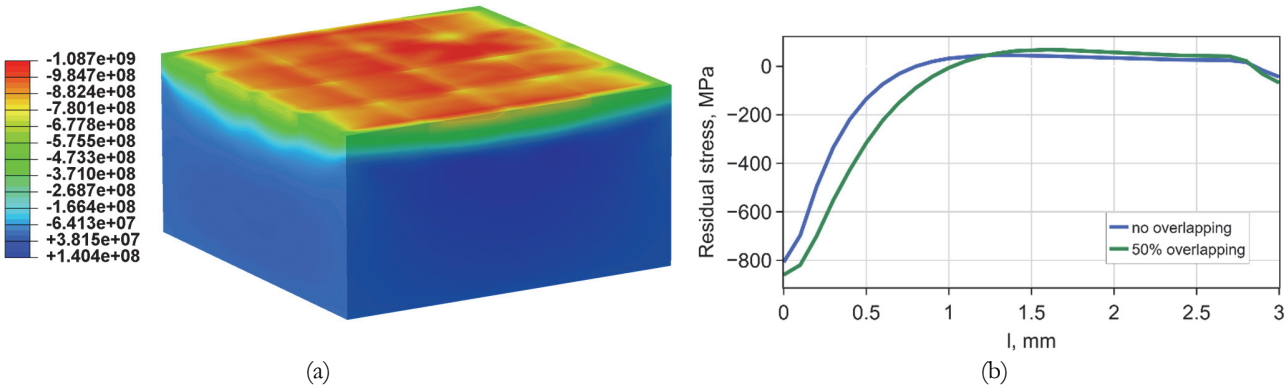

(a) (b)

Figure 8: (a) Residual stress distribution over the peened area and adjacent volume of the sample obtained by LSP with a peak intensity equal to 10 GW/cm² for square pulses of 3 mm and overlapping of 50%; (b) in-depth residual stress profiles obtained by LSP with and without overlapping, peak intensity equal to 10 GW/cm² and square pulses of 3 mm (blue line is no overlapping, green line is 50% overlapping).

Effect of spot shape

This section analyzes an effect of spot shape on the residual stress distribution. For this purpose, LSP by square spot with a size of 3 mm is compared with round spot having a diameter of 3 mm. In both cases, overlapping is 50% and peening strategy is the same as described in the previous section. The value of the peak intensity is equal to 10 GW/cm^2.

The residual stress distribution obtained by LSP with round spots shown in Fig. 9 (a). Similar to the results for the square spots presented in Fig. 8 (a) application of 50% overlapping allows one to level residual stress distribution at the surface of the sample although effect of the "residual stress hole" can be noted at the center of the each shot. It can be noted, that compressive residual stress on the surface peened by the round spot is lower than for square spots.

Fig. 9 (b) illustrates in-depth residual stress profiles for the considered cases. The results indicate that changing the shape of the spots does not modify considerably the residual stress profiles. There is only a slight decrease of 4% in the residual stress from -860 MPa to -895 MPa, when the square spot is changed to the round one. For both cases, the penetration depth is similar and is about 0.8 mm. The stress profiles are nearly the same. The most significant difference is only the absence of the compressive residual stress at the side opposite to the peened surface in the case of the round spot. Consequently, there is no significant difference in residual stresses obtained by LSP with square and round spots, when all other peeing parameters are the same.

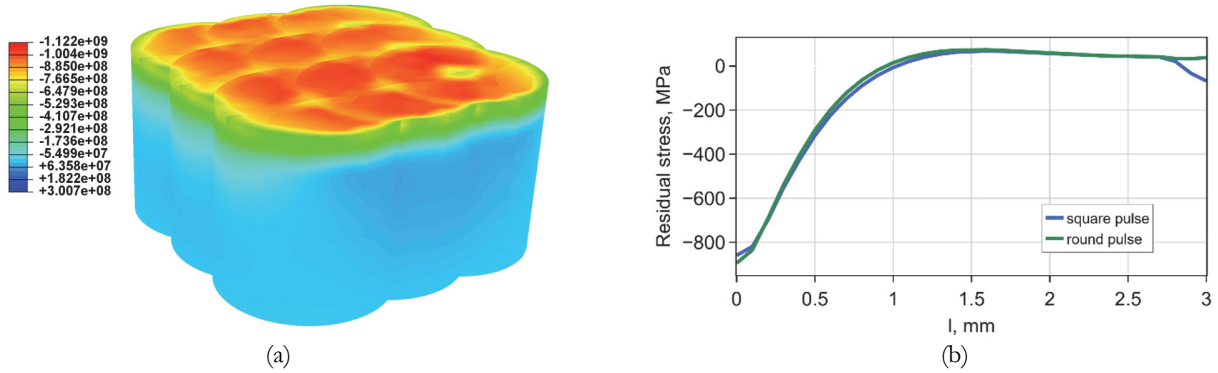

Figure 9: (a) Residual stress distribution over the peened area and adjacent volume of the sample obtained by LSP with a peak intensity equal to 10 GW/cm^2 for round pulses with diameter of 3 mm and overlapping of 50%; (b) in-depth residual stress profiles obtained by LSP with square and round spots and peak intensity equal to 10 GW/cm^2 (blue line is the square pulses with a size of 3 mm, green line is the round pulses with diameter of 3 mm).

Effect of pressure temporal variation

As it was mentioned above, there are several models of the temporal variation of the mechanical pressure induced by the expanding plasma. In general, the pressure pulse parameters and its duration depend on the laser used for LSP. In this section, we analyze residual stress resulting from three different pressure pulse shapes such as triangular, Gaussian and piece-wise linear. All considered pressure pulses are different from each other by qualitative temporal variation as well as by the impact duration. Thus, they can be considered as loading patterns resulting from LSP with three different lasers.

The triangular pulse is given by Eqn. (8). The Gaussian pulse normalized by a peak value is presented in Fig. 10 (a). It is similar to the pulse obtained from the problem of laser-matter-plasma interaction given in [13]. As it can be seen the pressure rises to its maximum value within the first 20 ns and then gradually decreases to zero from 20 ns to 300 ns. The linear piece-wise pulse approximation is shown in Fig. 10 (b). It is similar to the temporal variation given in [29]. As it is shown by the graph, the pressure pulse rises to its peak value during the first 3 ns. After that, in the following 3 ns the pressure amplitude is equal to the maximum value. Next, there is a downward trend which continues from 6 ns to 9 ns. In 9 ns the pulse value drops to 75% from the peak value. In 90 ns a more significant decline can be observed: the pressure value is equal to 30% of the maximum. From 90 ns to 170 ns the pressure remains steady. Finally, it plunges to 0.

Fig. 11 shows FEM results of LSP with the peak intensity equal to 10 GW/cm^2 and square pulses of 3 mm without overlapping for two temporal pressure variations given in Fig. 10. It can be seen, that periodic patterns of these distributions are similar. Near the peened surface of the sample a thin layer with compressive residual stress is formed. At the centers of each shot the magnitude of residual stress is lower than near the perimeter of the spot. However, the application of the dependence presented in Fig. 10 (a) results in a more uneven distribution at the surface than the dependence given in Fig. 10 (b). Moreover, the first pressure profile induces lower compressive residual stress than the second one. This is because

the maximum pressure in Fig. 10 (a) occurs later than in Fig. 10 (b). After reaching the peak the pressure declines steeper and the total duration of the pulse is two times larger than in Fig. 10 (b). It should be noted also that application of the triangular pulse (Fig. 4 (a)) shows less pronounced effect of "residual stress hole" in the center of the laser shot. Therefore, the different temporal pressure variations lead to the qualitative and quantitative distinctions in residual stress distributions.

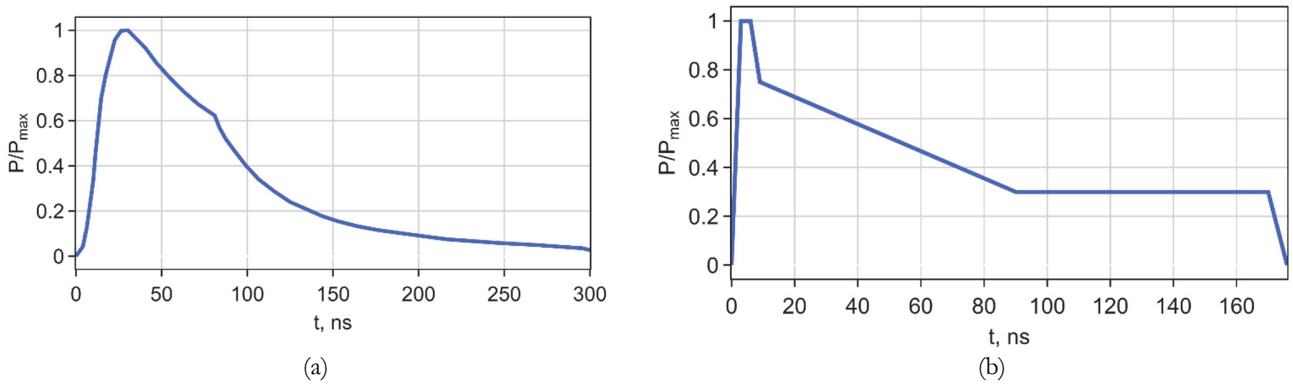

Figure 10: Temporal pressure variation: (a) Gaussian pulse similar to [13]; (b) piece-wise linear similar to [29].

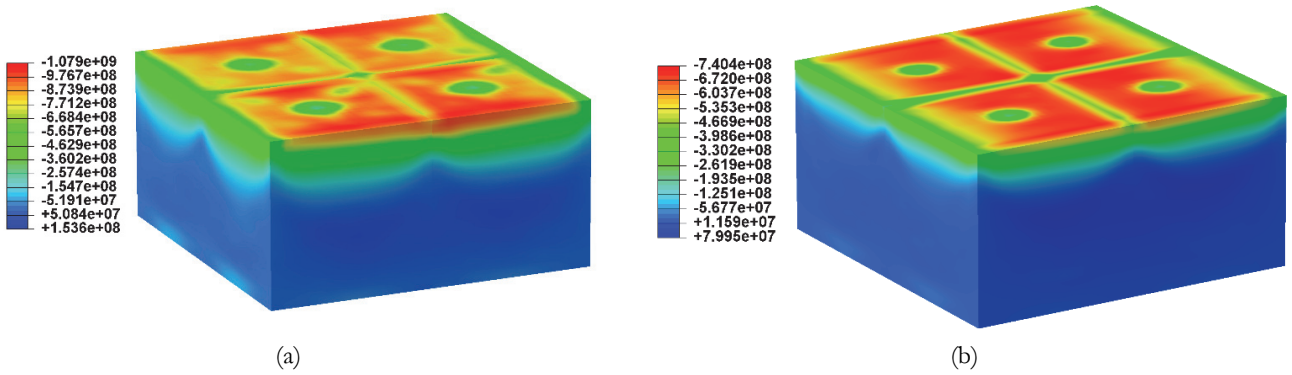

Figure 11: Residual stress distribution over the peened area and adjacent volume of the sample obtained by LSP with a peak intensity equal to 10 GW/cm² and square spots of 3 mm: (a) Gaussian temporal variation of pressure (Fig. 10 (a)); (b) Piece-wise linear temporal variation of pressure (Fig. 10 (b)).

Fig. 12 presents in-depth residual stress profiles for the three considered temporal pressure variations. The results illustrate that the pressure pulse given in Fig. 10 (b) produces the most moderate value of compressive residual stress at the peened surface of the specimen, which is equal to -580 MPa. The triangular and Gaussian pulses provide values closed to -800 MPa. Consequently, the application of the pulses described by Eqn. (8) and Fig. 10 (a) lead to an increase in the magnitude of surface residual stresses by 38%. Moreover, the second graph corresponding to the Gaussian pulse shows the most pronounced effect of "residual stress hole", which is indicated by a plateau from 0 to 0.1 mm. For the first and the third graphs this effect is not substantial.

It is worth mentioning that although the piece-wise linear pressure pulse produces a lower magnitude of the compressive residual stress at the peened surface than the triangular one, it leads to a higher penetration depth which is equal to 1.2 mm. In turn, the penetration depth for the triangular pulse is 0.8 mm. Due to the higher magnitude of the surface compressive residual stress, the application of the triangular pulse induces larger tensile residual stress in the mid-depth plane of the specimen, which are nearly zero for the piece-wise linear pulse. The largest penetration depth of 1.5 mm is obtained for the pressure pulse given in Fig. 10 (a). An increase in the penetration depth leads to the shift of the maximum tensile stress within the volume of the material to the side opposite to the peened area. It can be seen also that compressive residual stress at the opposite side significantly differs for the considered pressure pulses. The lowest value of -250 MPa is produced by the Gaussian pulse. The pulse of the piece-wise linear form gives the value of -160 MPa. The most insignificant compressive stress of -50 MPa corresponds to the triangular pulse.

The presented results have shown that the use of different temporal profiles of pressure pulses can lead to the qualitative and quantitative distinctions in the obtained residual stresses. Therefore, for the accurate description of residual stresses induced by LSP the precise form of the pressure temporal pulse should be established. Independent validation of this dependence can be made using the VISAR technique.

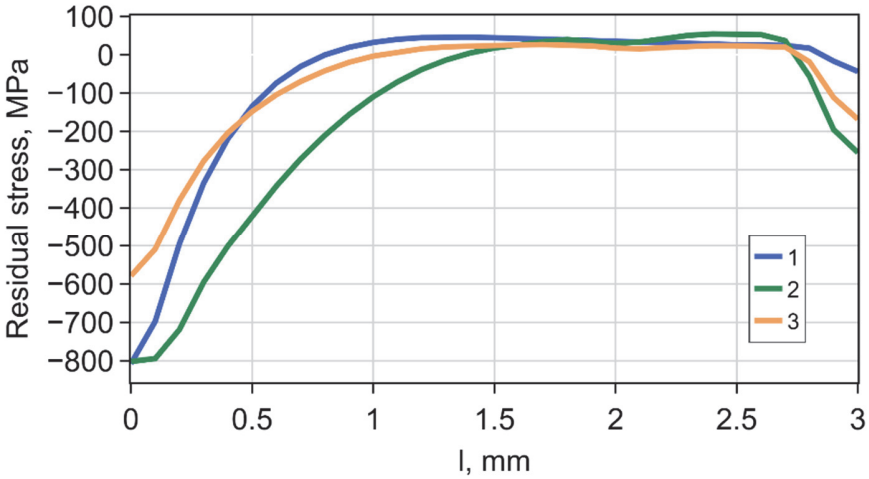

Figure 12: In-depth residual stress profiles obtained by LSP with square spots of 3 mm and peak intensity equal to 10 GW/cm² (1 is the triangular pressure pulse, 2 is the Gaussian pressure pulse similar to [13], orange line is the piece-wise linear similar to [29]).

Conclusion

This work is devoted to the finite-element study of residual stresses in Ti-6Al-4V plate induced by LSP with different parameters. For this purpose, a mathematical model of LSP was developed, calibrated and validated. The model neglects laser-matter interaction with subsequent plasma generation. Therefore, LSP is considered as a purely mechanical process where a plasma influence on the treated surface is taken into account by spatially uniform time-varying pressure pulse. The mathematical model is based on the strain rate sensitive Johnson-Cook constitutive equation. Material parameters were calibrated on the base of the experimental stress-strain curves obtained for the strain rates in the range of $5 \cdot 10^{-3} - 2.2 \cdot 10^{3}$ s^{-1}. In-depth finite-element residual stress profiles were verified by experimental data measured by hole drilling method for two spot sizes and several power densities. The calculated residual stresses were in a reasonable agreement with the experimental data under different LSP conditions.

Analysis of the peening parameters on residual stresses was performed by a series of numerical calculations for a plate of a thickness of 3 mm. The central region of the plate with dimensions of 6x6 mm was subjected to a sequence of laser shots with varying conditions. The following main conclusions can be drawn.

1) Larger spot sizes result in a more homogeneous residual stress distribution on the peened surface. Consequently, the magnitude of compressive residual stress at the surface and its penetration depth are higher. For the square spot with a size of 3 mm the rise in the magnitude and the penetration depth is 14 % and 33 %, respectively, in comparison with the spot of 1 mm under the identical other conditions. Therefore, for the same power densities, it is preferable to use larger spot sizes.

2) A rise in the pulse energy induces an increase in the magnitude of compressive residual stress at the peened surface of the sample. However, the magnitude of the residual stress changes non-linearly and tends to saturation, such that each subsequent increase in the pulse energy produces a lower increment of the magnitude. The same conclusion can be drawn for the penetration depth of the compressive residual stress. The rise in the pulse energy from 5J to 7J resulted in increase of the compressive stress magnitude by 70% and the subsequent rise to 9J increased the surface magnitude only by 18%. The increase in the penetration depth is 40 % for the rise in energy from 5J to 7 J and 14% for the rise from 7J to 5J. This conclusion indicates that in order to obtain acceptable compressive residual stresses with the use of a high-power laser it is not always required to apply its maximum energy.

3) LSP conducted by two peen layers can improve the magnitude of compressive residual stress and its penetration depth. However, extra layers do not lead to a significant improvement of LSP results. The second peen layer gains the magnitude of the compressive residual stress at the peened surface by 11.2% and increases the penetration depth by 25%. For the third

peen layer, these values rise by 4.5 and 15%, respectively. Hence, enhancement of the compressive residual stress in the sample by adding extra peen layers is also limited by the saturation effect.
4) LSP with shots overlapping shows more uniform residual stress distribution than LSP without overlapping. However, peening with 50% overlapping doesn't lead to a substantial improvement of compressive residual stress, which magnitude growth is only 7.5%. Although the compressive residual stress magnitude is almost the same, 50% overlapping increases the penetration depth by 37.5 %. Therefore, the strategy of peening with shots overlapping leads to the generation of deeper compressive residual stresses. This effect is important for a? fatigue life improvement of materials because cracks are formed in a subsurface zone.
5) The shape of the laser spots has the least effect on the in-depth residual stress profiles among the all considered LSP conditions. The use of a round spot increases the surface residual stress magnitude only by 4% in comparison with square pulses while the penetration depth doesn't change. Therefore, there is no difference in the application of square or round spots when LSP with 50% overlapping is conducted. However, for the LSP without overlapping the square pulse is preferred since its cover all peening area and thus, provides a more uniform distribution of the residual stress field.
6) Temporal variation of the pressure pulse substantially affects the obtained results. Three of the most used types of pressure pulses considered in the paper (triangular, Gaussian and piece-wise linear) show a different qualitative and quantitative influence on the surface residual stress distribution and in-depth residual stress profiles. Application of the Gaussian pulse results in the most uneven residual stress distribution on the peened surface and characterizes the most pronounced effect "residual stress hole". Also, the triangular and Gaussian pulses induce nearly the same value of the surface compressive stress magnitude, while the piece-wise linear gives the value of 38% lower. Despite the similar surface compressive residual stresses, the Gaussian and triangular pulses are characterized by the different penetration depth. The penetration depth for the Gaussian pulse is 87.5% higher than that of the triangular one. The penetration depth for the piece-wise linear pulse is larger than for the triangular pulse by 50%. Therefore, the laser shots with the triangular pulse causes the residual stresses at the humbler depth among the considered pulses. These results indicate, that the use of different lasers with the same power density can lead to distinct in-depth residual stress profiles.
7) Among the all considered peening parameters, the most substantial effect on the numerical results has a pulse energy. Also, significant alteration of the in-depth residual stress profiles and the penetration depth can be observed for different temporal pulse variations. In addition, the use of the larger spot size and 50% shots overlapping can remarkably improve the penetration depth. The least significant parameter which almost has no influence on the residual stress profiles is the pulse shape.

Acknowledgments

The reported study was supported by the Government of Perm Krai, research project No. C-26/829.

References

[1] Kashaev, N., Ventzke, V., Horstmann, M., Chupakhin, S., Riekehr, S., Falck, R., Maawad, E., Staron, P., Schell, N. and Huber, N. (2017). Effects of laser shock peening on the microstructure and fatigue crack propagation behavior of thin AA2024 specimens, Int. J. Fatigue, 98, pp. 223-233. DOI: 10.1016/j.ijfatigue.2017.01.042.
[2] Pavan, M., Furfari, D., Ahmad, B., Gharghouri, M. and Fitzpatrick, M. (2019) Fatigue crack growth in a laser shock peened residual stress field, Int. J. Fatigue, 123, pp. 157-167. DOI: 10.1016/j.ijfatigue.2019.01.020.
[3] Hu, Y., Cheng, H., Yu, J. and Yao, Z. (2020). An experimental study on crack closure induced by laser peening in pre-cracked aluminum alloy 2024-T351 and fatigue life extension, Int. J. Fatigue, 130, 105232. DOI: 10.1016/j.ijfatigue.2019.105232.
[4] Hassan, S.S., Hamzah, M.N. and Abed, R.M. (2018). The effect of laser shock peening on fatigue life using pure water and hydrofluoric acid as a confining layer of Al–alloy 7075-T6, J. Eng., 24(1), pp. 207–217.
[5] Clauer, A.H., Fairand, B.P. and Slater, J.E. (1977). Laser shocking of 2024 and 7075 aluminum alloys, Technical Report, Battelle Columbus Labs, OH, United States.

[6] Navarro, C., Vázquez, J. Domínguez, J., Periñán, A., García, M. H., Lasagni, F., Bernarding, S., Slawik, S., Mücklich, F., Boby, F. and Hackel, L. (2020) Effect of surface treatment on the fatigue strength of additive manufactured Ti6Al4V alloy, Frat. ed Integrita Strutt., 53, pp. 337-344. DOI: 10.3221/IGF-ESIS.53.26.
[7] Braisted, W. and Brockman, R. (1999). Finite element simulation of laser shock peening, Int. J. Fatigue, 21, pp. 719-724. DOI: 10.1016/S0142-1123(99)00035-3.
[8] Keller, S., Chupakhin, S., Staron, P., Maawad, E., Kashaev, N. and Klusemann, B. (2018). Experimental and numerical investigation of residual stresses in laser shock peened AA2198, J. Mater. Process. Technol., 255, pp. 294-307. DOI: 10.1016/j.jmatprotec.2017.11.023.
[9] Peyre, P., Berthe, L., Vignal, V., Popa, I. and Baudin, T. (2012). Analysis of laser shock waves and resulting surface deformations in an Al-Cu-Li aluminum alloy, J. Phys. D Appl. Phys., 45, 335304. DOI: 10.1088/0022-3727/45/33/335304.
[10] Langer, K. and Spradlin, T.J, Fitzpatrick, M. E. (2020). Finite element analysis of laser peening of thin aluminum structures, Metals, 10, 93. DOI:10.3390/met10010093.
[11] Kim, R., Suh, J., Shin, D., Lee, K.-H., Bae, S.-H., Cho, D.-W., Yi, W.-G. (2021). FE Analysis of laser shock peening on STS304 and the effect of static damping on the solution, Metals, 11, 1516. DOI: 10.3390/met11101516.
[12] Sticchi, M., Staron, P., Sano, Y., Meixer, M., Klaus, M., Rebelo-Kornmeier, J., Huber, N. and Kashaev, N. (2015). A parametric study of laser spot size and coverage on the laser shock peening induced residual stress in thin aluminium samples, J. Eng., 13, pp. 1-9. DOI: 10.1049/joe.2015.0106.
[13] Pozdnyakov, V., Keller, S., Kashaev, N., Klusemann, B. and Oberrath, J. (2022). Coupled modeling approach for laser shock peening of AA2198-T3: from plasma and shock wave simulation to residual stress prediction, Metals, 12, 107. DOI: 10.3390/met12010107.
[14] Hfaiedh, N., Peyre, P., Song, H., Popa, I. and Ji, V. (2015). Finite element analysis of laser shock peening of 2050-T8 aluminum alloy, Int. J. Fatigue, 70, pp. 480-489. DOI: 10.1016/j.ijfatigue.2014.05.015.
[15] Golabi, S., Vakil, M.R., Amirsalari, B. (2019). Multi-objective optimization of residual stress and cost in laser shock peening process using finite element analysis and PSO algorithm, Lasers Manuf. Mater. Process., 6, pp. 398–423. DOI: 10.1007/s40516-019-00102-1.
[16] Wang, C., Li, K., Hu, X., Yang, H. and Zhou, Y. (2021). Numerical study on laser shock peening of TC4 titanium alloy based on the plate and blade model, Opt. Laser Technol., 142, 107163. DOI: 10.1016/j.optlastec.2021.107163.
[17] Zhang, X., Li, H., Duan, S., Yu, X., Feng, J., Wang, B. and Huang, Z. (2015). Modeling of residual stress field induced in Ti–6Al–4V alloy plate by two sided laser shock processing, Surf. Coat. Technol., 280, pp. 163-173. DOI: 10.1016/j.surfcoat.2015.09.004.
[18] Xu, G., Luo, K. Y., Dai, F. Z. and Lu, J.Z. (2019). Effects of scanning path and overlapping rate on residual stress of 316L stainless steel blade subjected to massive laser shock peening treatment with square spots, Appl. Surf. Sci., 481, pp. 1053-1063. DOI: 10.1016/j.apsusc.2019.03.093.
[19] Hu, Y., Gong, C., Yao, Z. and Hu, J. (2009). Investigation on the non-homogeneity of residual stress field induced by laser shock peening, Surf. Coat. Technol., 203, pp. 3503-3508. DOI: 10.1016/j.surfcoat.2009.04.029.
[20] Mylavarapu, P., Bhat, C., Reddy Perla, M. K., Banerjee, K., Gopinath, K. and Jayakumar, T. (2021). Identification of critical material thickness for eliminating back reflected shockwaves in laser shock peening – A numerical study, Opt Laser Technol., 142, 107217. DOI: 10.1016/j.optlastec.2021.107217.
[21] Ding., K. and Ye, L. (2006). Laser Shock Peening: Performance and Process Simulation, Cambridge, Woodhead. Publishing Limited.
[22] Amarchinta, H. (2010). Uncertainty quantification of residual stresses induced by laser peening simulation, PhD Dissertation in Engineering, Dayton, Wright State University.
[23] Langer, K., Olson, S., Brockman, R., Braisted, W., Spradlin, T., and Fitzpatrick, M. E. (2015). High strain-rate material model validation for laser peening simulation, J. Eng., 13, pp. 150-157. DOI: 10.1049/joe.2015.0118.
[24] Amarchinta, H. K., Grandhi, R. V., Clauer, A. H., Langer, K., and Stargel, D. S. (2010). Simulation of residual stress induced by a laser peening process through inverse optimization of material models. J. Mater. Process. Technol., 210(14), pp. 1997-2006. DOI: 10.1016/j.jmatprotec.2010.07.015.
[25] Li, X., He, W., Luo, S., Nie, X., Tian, L., Feng, X. and Li, R. (2019). Simulation and experimental study on residual stress distribution in titanium alloy treated by laser shock peening with flat-top and Gaussian laser beams, Materials, 12, 1343. DOI: 10.3390/ma12081343.
[26] Warren, A. W., Guo, Y. B. and Chen, S. C. (2008). Massive parallel laser shock peening: Simulation, analysis, and validation, Int. J. Fatigue, 30, pp. 188-197. DOI: 10.1016/j.ijfatigue.2007.01.033.

[27] Hu Y., Yao Z. (2008). Numerical simulation and experimentation of overlapping laser shock processing with symmetry cell, Int. J. Mach. Tools Manuf., 48, pp. 152-162. DOI: 10.1016/j.ijmachtools.2007.08.021.
[28] Zhao, J., Dong, Y. and Ye, C. (2017). Laser shock peening induced residual stresses and the effect on crack propagation behavior, Int. J. Fatigue, 100, pp. 407-417. DOI: 10.1016/j.ijfatigue.2017.04.002.
[29] Nam, T. (2002). Finite element analysis of residual stress field induced by laser shock peening, PhD Dissertation in Mechanical Engineering, Columbus: Ohio State University.
[30] Fabbro, R., Fournier, J., Ballard, P., Devaux, D. and Virmont, J. (1990). Physical study of laser-produced plasma in confined geometry, J. Appl. Phys., 68, pp. 775-784. DOI: 10.1063/1.346783.